ACS APPLIED MATERIALS & INTERFACES

Research Article

www.acsami.org

Engineered Nanostructured Facial Lipopeptide as Highly Efficient Molecular Transporter

Chiranjit Dutta,[#] Kasturee Chakraborty,[‡] and Rituparna Sinha Roy*[,‡]

[#]Department of Chemical Sciences and [‡]Department of Biological Sciences, Indian Institute of Science Education and Research Kolkata, Mohanpur 741246, West Bengal, India

Supporting Information

ABSTRACT: Designing an effective peptide based molecular transporter for the intracellular delivery of hydrophilic therapeutic biomacromolecules remains a considerable challenge. Highly basic oligoarginine and lipidated arginine rich cell penetrating peptides have been reported in the literature as molecular transporters, which were extensively used for cellular internalization of significantly large biopharmaceuticals. However, oligoarginine based molecular transporters with L-arginine residues pose significant challenges due to proteolytic instability and limited stability of noncovalent peptide−cargo nanocomplexes. Exploiting the rational peptide designing strategy, we have engineered protease-resistant facial lipopeptide based molecular transporter having arginine-sarcosine-arginine moiety to minimize adjacent arginine-arginine pair repulsion. N-Methylated amino acid sarcosine was incorporated as a spacer between two adjacent arginine residues, which provides proteolytic stability to the designed peptide and minimizes intermolecular aggregation of peptides. Two stearyl moieties were incorporated to facilitate cellular internalization. Interestingly, our designed lipopeptide exhibits significantly enhanced cellular internalization with only six L-arginine residues compared to stearylated oligo-nona-arginine. Additionally, enhanced proteolytic stability of such class of molecular transporter enables increased cargo internalization, and we anticipate that our engineered multifunctional, proteolytically stable, nanostructured facial lipopeptide based molecular transporter can have major impact in advancing drug delivery technologies.

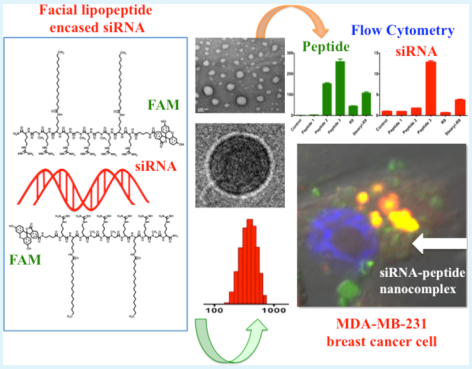

KEYWORDS: *peptides, molecular transporter, drug delivery, nanoparticle, biopharmaceuticals, lipopeptide*

1. INTRODUCTION

The intracellular delivery of hydrophilic macromolecules remains a significant challenge to the pharmaceutical industry.[1−5] The existing cellular internalization delivery methods pose substantial challenges owing to the limited stability of vehicles and vehicle−cargo complexes.[1] Synthetic polymer, lipid, and peptide based carriers have facilitated the delivery of biopharmaceuticals primarily aimed at extracellular targets.[6] Efforts need to be focused on developing improved drug delivery materials that enable high yield intracellular delivery of macromolecules in functionally active form.

Among the major avenues of the noninvasive intracellular delivery of therapeutic macromolecules, cell-penetrating membrane permeable cationic peptides and proteins are extensively harnessed as promising molecular transporters.[3,7,8] The delivery technology of therapeutic molecules can follow either covalent or noncovalent cell penetrating peptide based strategy.[3] For certain cargos, noncovalent strategies appear to be more appropriate, as they promotes the delivery of cargo in functionally active form and yield enhanced biological responses.[3] Both oligoarginine and amphipathic membrane permeable peptides were used for intracellular delivery of biologically active cargos.[3,8] From a structural point of view, several groups have examined the efficiency of molecular transporters having unstructured and structured backbones. Additionally, the role of backbone spacing between two adjacent cationic residues and the need for different categories of lipids for lipid modification of molecular transporters were also evaluated. The groups of Parang, Cardoso, and Pei have demonstrated that cyclic peptides can act as efficient molecular transporters[9−11] and backbone rigidity and static presentation of guanidinium groups increase the cellular uptake of arginine rich membrane permeable peptides.[10] Besides using constrained peptide backbones, cellular uptake can also be enhanced by conjugating lipidic moieties with peptide transduction domains.[12−14] Apart from using shorter peptides, several groups have examined the role of proteins as molecular transporters. Well-folded minimally cationic miniature proteins have also been used as molecular transporters, which follow a desired delivery pathway for rapid cytosolic access and are capable of modulating protein function at cytoplasm.[15,16] Liu and co-workers have used supercharged green fluorescent protein for delivering nucleic acid reagents to mammalian cell line which is resistant to cationic lipid-mediated siRNA

Received: May 21, 2015
Accepted: August 4, 2015
Published: August 4, 2015

DOI: 10.1021/acsami.5b04392
ACS Appl. Mater. Interfaces 2015, 7, 18397−18405

transfection.[17] Besides, examining the role of constrained and unconstrained shorter peptides and functionalized proteins as molecular transporters, the necessity of using a spacer between two cationic moieties was also examined. Lehto et al. has shown that stearylated $(Arg\text{-}Xxx\text{-}Arg)_4$ peptide shows efficient delivery of nucleic acids by noncovalent strategy and backbone spacing amplifies the efficiency of molecular transporters.[18] Additionally, it is also reported that amphipathic peptides are more potent than oligocationic peptides as cell internalizers.[19−21]

Among cationic peptides, arginine rich peptides are having the best cell penetrating efficiency[22−24] due to the physicochemical feature of the highly basic guanidino group of arginine side chain which facilitates enhanced cellular uptake compared to the lysine and histidine residues by forming stronger bidentate hydrogen bonds with cell surface phosphates, sulfates, and carboxylates.[7,25] The length dependence studies of oligoarginine peptides have shown that oligoarginine peptides having eight to nine arginine residues have the best cell-penetrating efficiency.[23] Lipid modification of oligoarginine peptide facilitates cellular internalization and among stearyl, lauryl, cholesteryl, and cholyl hydrophobic moieties, with the stearyl moiety showing the best transfection efficiency.[23] Interestingly, besides amphipathic peptides, peptides having spacing between adjacent arginine residues have shown better internalization efficiency compared to oligoarginine peptides, suggesting that the Arg-Xxx-Arg motif facilitates the internalization and promotes the stability of peptide−cargo complex by reducing the adjacent Arg-Arg pair repulsion.[18,19]

Traditional oligocationic peptide based molecular transporters with L-amino acids demonstrate significant challenges due to reduced proteolytic stability against cellular trypsin like proteases and limited stability of transporter-cargo noncovalent complexes.[18] To address these issues, exploiting the amphipathic peptide scaffold arginine-sarcosine-arginine as template, we have engineered doubly stearyl functionalized L-arginine rich protease-resistant facial lipopeptide which demonstrated significantly enhanced cellular internalization of peptides and peptide-cargo complexes with six L-arginine residues. We find that incorporation of unnatural residue, sarcosine as a spacer between two adjacent Arg residues has provided proteolytic stability to our designed sequences, inhibited the extensive intermolecular association and stabilized the peptide−cargo complexes. We report that Arg-Xxx-Arg template containing sequences significantly stabilizes peptide−cargo complexes compared to oligoarginine sequences and shows better internalization ability due to proteolytic stability. Additionally, the less cationic charge in peptides can potentially facilitate the internalized peptide−cargo nanocomplex unpacking at acidic pH.

2. MATERIALS AND METHODS

Materials. All Fmoc protected amino acids and resins were purchased from Novabiochem and G L Biochem and used without further purification. The coupling reagent (2-(1*H*-benzotriazol-1-yl)-1,1,3,3-tetramethyluronium hexafluorophosphate) (HBTU) and (benzotriazol-1-yl-oxytripyrrolidinophosphonium hexafluorophosphate) (PyBOP) were purchased from Novabiochem, and hydroxybenzotriazole (HOBt) was purchased from SRL (Sisco Research Laboratoratories Pvt. Ltd.). The anhydrous dimethylformamide (DMF) and dichloromethane (DCM) were purchased from Acros Organics, and anhydrous *N*,*N*-diisopropylethylamine (DIPEA), dimethyl sulfoxide (DMSO), stearic acid, and 2,4,6-trinitrobenzenesulfonic acid (TNBS) were obtained from Sigma-Aldrich. 5(6)-Carboxyfluorescein and Hiperfect were purchased from Invitrogen. siGLO Red Transfection reagent (DY-547 labeled siRNA) was procured from Dharmacon. All procured chemicals have ∼98−99% purity.

Synthesis of Lipopeptides. All peptides were synthesized by Fmoc solid phase peptide synthesis strategy. The successive coupling of stearic acid was done after deprotection of mild acid labile 4-methyltrityl (Mtt) group from Fmoc-Lys(Mtt)-OH by 1% TFA/5% TIS/DCM for 1 h followed by coupling using 6 equiv of stearic acid, PyBOP (6 equiv), HOBt (6 equiv), and DIPEA in DMF/DCM (1:1) for 12 h at room temperature (Scheme S1, Supporting Information). The attachment of 5(6)-carboxyfluorescein (FAM) was done by using 10 equiv of FAM, HOBt, PyBOP, and DIPEA in DMF for 12 h at room temperature to yield FAM-labeled peptide. The peptides were purified by HPLC using C18 column and confirmed by MALDI-TOF mass spectra (Table S1, Figure S1−S5) and NMR spectra (Figure S6−S7).

Circular Dichroism. Circular dichroism (CD) spectra were recorded on a JASCO spectrometer using a cell of 1 mm path length. Peptides were dissolved in 25 mM phosphate buffer having pH 7.4 and peptide concentrations used were 60−110 μM and CD spectra were recorded in the range of 195−240 nm wavelength. CD spectra were obtained as accumulation of three scans using a scan speed of 100 nm/min, data pitch of 0.2 nm and bandwidth 1.0 nm. Each spectrum was subtracted from the buffer and smoothened and plotted using Origin Pro 8.

Dynamic Light Scattering. The hydrodynamic radius and zeta potential were measured using dynamic light scattering instrument (Zetasizer-Nano, Malvern, Inc.). The hydrodynamic radius of peptide and peptide−siRNA nanocomplexes were prepared in RNase free water. The measurements were carried out in triplicate. Size and zeta potential data were plotted using GraphPad prism and values are represented as mean ± SD of three independent experiments.

Transmission Electron Microscopy (TEM). The TEM sample was prepared for peptide−siRNA complex (100:1 ratio) in RNase free water on a freshly glow-discharged carbon coated 300 mesh copper grid. A volume of 5 μL of sample solution was drop-casted on the copper grid and incubated for 5 min at room temperature. The excess solution was wiped out and washed with water and stained with 2% uranyl acetate. The morphology of peptide and peptide-siRNA complexes were characterized by using a Tecnai G2 F20 ST transmission electron microscope (FEI Company) with accelerating voltages of 120 and 200 kV.

Cryogenic Transmission Electron Microscopy (Cryo-TEM). Peptide 3−siRNA complex was spread on glow-discharged 300 mesh carbon coated Cu grids and plunge-frozen in liquid ethane using Vitrobot (FEI company). Grids were transferred to a cryoholder and visualized in Tecnai POLARA (FEI Company) equipped with 300 kV field emission gun (FEG). Images were collected at 82 600× magnification with an underfocus of 5 μm. Images were captured on an Eagle 4 k × 4 k CCD camera (FEI Company) unbinned with a final pixel size of 1.85 Å.

Scanning Electron Microscopy. The peptide samples (500 μM) and peptide−siRNA complexes (100:1) were coincubated with 2% glutaraldehyde in RNase free water at 4 °C for overnight. A drop containing 10 μL of sample was placed on a glass coverslip and allowed to semidry in air. Next hexamethyldisilazane (HMDS) was added and the sample was dried by evaporating HMDS, which is considered as good alternative of critical point drying. The samples on glass were coated using gold−palladium and were analyzed using SUPRA 55VP-field emission scanning electron microscope (Zeiss company). This instrument has high performance variable pressure FE-SEM with patented GEMINI column technology, Schottky type field emitter system, single condenser with crossover-free beam path, resolution: 1.0 nm at 15 kV; 1.6 nm at 1 kV high vacuum mode; and 2.0 nm at 30 kV at variable pressure mode.

Protease Stability of Peptides. The protease stability of peptides were carried out in the presence of trypsin protease. In general, 0.1 μg of trypsin was taken in 150 μL of PBS buffer (pH 7.5, 10 mM phosphate buffer, 150 mM NaCl) and 0.2 mM FAM labeled peptide was mixed and resulting solution was incubated at 37 °C. A volume of

DOI: 10.1021/acsami.5b04392
ACS Appl. Mater. Interfaces 2015, 7, 18397−18405

10 μL of digestion mixture was periodically taken out for 48 h and then quenched with 0.2% trifluoroacetic acid and immediately frozen in liquid nitrogen and stored at −20 °C before using for MALDI-TOF analysis.

Gel Retardation Assay. To study the ability of peptide 3 to coassemble with siRNA, agarose gel electrophoresis was carried out at 80 V for 60 min in TAE buffer (2 M Tris base, 1 M glacial acetic acid, 0.5 M sodium EDTA, pH 8.3). Peptide 3 and siRNA were mixed at different ratios ranging from 1:5 to 1:100 and incubated at 37 °C for 20 min to form complexes. Samples were loaded onto a 2% wt/vol agarose gel and stained with 0.5 μg/mL ethidium bromide with 6× loading buffer, and then siRNA bands were visualized using an UV (ultraviolet) imaging system (GOLD-SIM).

Cell Culture. Human breast adenocarcinoma cells (MDA-MB-231) were cultured in Dulbecco's modified Eagle's medium (DMEM, purchased from invitrogen) with 10% bovine serum (Gibco) and 1% penicillin−streptomycin.

Cell Viability Assay. The toxicity studies of the peptides were carried out by using the cell viability assay (MTT assay). Human breast adenocarcinoma cells (MDA-MB-231) were seeded (10 000 cell/well) in 96-well plates and kept overnight for growing. The media was removed, and the cells were incubated with different concentrations of peptides (500 nM, 2 μM, 5 μM, and 10 μM) in DMEM media at 37 °C for 24, 48, and 72 h. Each condition was taken in triplicate. After 24−72 h, the peptide containing media was removed and washed with PBS, and then a mixture of 10 μL of 5 mg/mL MTT solution (3-(4,5-dimethylthiazol-2-yl)-2,5-diphenyltetrazolium bromide) and 90 μL of phenol-red free DMEM media were added in each well of the 96-well plate and incubated for 3 h. Then 150 μL of DMSO was added to dissolve the formazan crystal and the absorbance was measured at 570 nm. MTT data were plotted using GraphPad Prism, and values are represented as mean ± SD of three independent experiments.

Cellular Uptake Studies Using Flow Cytometry Instrument. *Time Dependent Cellular Uptake Studies.* Human breast adenocarcinoma cells (MDA-MB-231) were grown in six-well plates (1×10^6 cells/well) in DMEM media and incubated with 5 μM 5(6)-carboxyfluorescein (FAM) labeled peptides for different incubation times (5, 60, and 180 min) in Opti-MEM media at 37 °C in an incubator supplied with 5% CO_2. DMSO and FAM were taken as control. The cells were digested with 0.25% trypsin in EDTA for 5 min to detach the cells as well as the surface bound peptides followed by washing two times with ice cold PBS, resuspended in ice cold PBS with 5% FBS, and then analyzed by flow cytometry (BD FACSVerse, San Jose, CA). The PMT voltage was optimized with the unstained sample. The same PMT voltage, threshold, and other parameters were used throughout the experiment. A minimum of 10 000 cells were analyzed for each sample. The experiments were performed in triplicate. The FAM is excited by 488 nm laser, and emission signal is collected using 527/32 band-pass filter. The flow cytometry data was analyzed using BD FACSuite software (v.1.0.5, San Jose, CA). The flow cytometry data was further analyzed using GraphPad Prism software. The results are represented as mean ± SD of three independent experiments.

Effect of Energy Depletion on Cellular Uptake. We performed the cellular uptake studies in the presence of inhibitors (10 mM NaN_3 and 50 mM 2-deoxy-D-glucose), which induce ATP depletion in the cells. To probe whether peptide trafficking involves energy-independent or energy-dependent pathway, we treated the cells with 10 mM NaN_3 and 50 mM 2-deoxy-D-glucose for 30 min at 37 °C to induce ATP depletion. Without removing the media, the cells were treated with 5 μM FAM labeled peptides for 1 h at 37 °C. The cells were trypsinized and the flow cytometry protocol was followed as mentioned above. The flow cytometry data was plotted using GraphPad Prism and values are represented as mean ± SD of two independent experiments.

Effect of Inhibitors on Cellular Uptake. Human breast adenocarcinoma cells (MDA-MB-231) were grown in six well plates (1×10^6 cells/well) in DMEM media. The cells were incubated with different inhibitors of endocytosis (chlorpromazine, methyl-β-cyclodextrin, 5-(*N*-ethyl-*N*-isopropyl)amiloride and Nystatin) and actin polymerization inhibitor (cytochalsin D) in Opti-MEM media at 37 °C for 30 min. Next, 30 μM chlorpromazine, 2.5 mM methyl-β-cyclodextrin, 50 μM 5-(*N*-ethyl-*N*-isopropyl)amiloride, 50 μg/mL Nystatin, and 10 μg/mL cytochalsin D were used followed by incubation with 5 μM FAM labeled peptides for 1 h at 37 °C incubator. Cells incubated with 5 μM FAM labeled peptides for 1 h at 37 °C were used as controls. The cells were trypsinized, and the flow cytometry protocol was followed as mentioned above. The flow cytometry data was plotted using GraphPad Prism and values are represented as mean ± SD of two independent experiments.

Cellular Uptake Studies of Peptide−Cargo Complex. Human breast adenocarcinoma cells (MDA-MB-231) were grown in six well plates (1×10^6 cells/well) in DMEM media. DY-547 labeled siRNA, which is an siGLO red transfection indicator, was used as labeled cargo. The cells were incubated with peptide−siRNA complex (100:1 ratio) for 1 h in a 37 °C incubator. The peptide−siRNA complex was incubated for 30 min before adding to the cells. The flow cytometry data of FAM labeled peptides and siRNA−Hiperfect mixture were used for FITC and TRITC signal compensation, respectively. The cells were trypsinized, the flow cytometry protocol was followed as mentioned above, and analysis was carried out using FITC and PE channel. The FAM (FITC) is excited by 488 nm laser, and emission signal is collected using a 527/32 band-pass filter. PE (TRITC) is excited by 488 nm laser, and emission signal is collected using a 586/42 band-pass filter. The flow cytometry data was plotted using GraphPad Prism, and values are represented as mean ± SD of three independent experiments.

Uptake Studies by Confocal Microscopy. *Cellular Uptake Studies of Peptides.* MDA-MB-231 cells (50 000 cells) were seeded on coverslips in 24-well plates and treated with 5 μM peptide for 1 h at 37 °C. The media was removed, and cells were washed twice and fixed with 3.5% paraformaldehyde. The nuclei were stained wih 4′,6-diamidino-2-phenylindole (DAPI) and finally washed with PBS. The coverslips were mounted on microscope slides with mounting media upside down and observed under a Zeiss LSM 710 confocal microscope. Images were taken in Plan Apochromat 63× oil immersion objectives with N.A. 1.4. Zen 2010 software was used for acquisition and processing of the data.

Effect of Energy Depletion on Cellular Uptake. For uptake studies, in the presence of NaN_3 and 2-deoxy-D-glucose, cells were incubated with 10 mM NaN_3 and 50 mM 2-deoxy-D-glucose for 30 min at 37 °C followed by incubation with 5 μM FAM labeled peptides for 1 h at 37 °C. The cells were fixed, and nuclei were stained with DAPI as mentioned above and observed under confocal microscope.

Effect of Inhibitors on Cellular Uptake. For uptake studies in the presence of inhibitors, cells were incubated with 5 μg/mL chlorpromazine, 2.5 mM methyl-β-cyclodextrin, 50 μM 5-(*N*-ethyl-*N*-isopropyl) amiloride (EIPA), and 10 μg/mL Cytochalasin D for 30 min followed by incubation with 5 μM peptides for 1 h at 37 °C. The cells were fixed and nuclei were stained with DAPI as mentioned above and observed under confocal microscope.

Cellular Uptake Studies of Peptide−Cargo Complexes. DY-547 labeled siRNA, which is siGLO red transfection indicator was used as labeled cargo. For uptake studies in the presence of peptide−siRNA nanocomplexes, cells were treated with a mixture of 5 μM FAM labeled peptides and 50 nM DY-547 labeled siRNA for 1 h at 37 °C. The media was removed, and cells were washed twice and fixed with 3.5% paraformaldehyde. The cells were fixed and nuclei were stained with DAPI as mentioned above and observed under confocal microscope.

Release of Cargo and Peptide from Peptide−Cargo Nanocomplexes with Time. MDA-MB-231 cells were treated with a mixture of 5 μM FAM labeled peptide and 50 nM DY-547 labeled siRNA for 1 h at 37 °C. The media was removed, cells were washed after 1 h, and then cells were kept in Opti-MEM media. Cells were fixed with 3.5% paraformaldehyde at 1, 3, and 6 h time points after removing the media, and nuclei were stained with DAPI as mentioned above and observed under confocal microscope.

DOI: 10.1021/acsami.5b04392
ACS Appl. Mater. Interfaces 2015, 7, 18397−18405

3. RESULTS AND DISCUSSION

Peptide Design. Our key focus is to design short proteolytically stable L-arginine rich molecular transporter for delivering hydrophilic therapeutic biomacromolecules. Toward the goal, we designed three arginine-rich peptide sequences, peptides 1−3, as described in Table 1. Figure 1 shows the schematic diagram of peptide 3. Our designed peptides have the following features: (a) alternate hydrophilic and hydrophobic residues to confer facial amphiphilicity; (b) side chain modification by stearyl moiety to increase hydrophobicity, a modification important for cellular internalization;[18,23,26] (c) incorporation of *N*-methylglycine (sarcosine, abbreviated as "Sar" in Table 1) to enhance proteolytic stability against cellular trypsin-like proteases and also to promote the solubility of the designed sequences by inhibiting interpeptide self-assembly due to the absence of amide proton in sarcosine;[27] (d) Arg-Xxx-Arg motif to increase the peptide−cargo stability by reducing adjacent Arg-Arg repulsion; (e) γ-aminobutyric acid (γAbu) incorporated as spacer between carrier peptide segment and fluorescein moiety (FAM); and (f) FAM incorporated as fluorophore for flow cytometry and microscopic studies. Peptides Arg9 (abbreviated as R9) and stearyl-Arg9 (abbreviated as stearyl-R9) were also synthesized as control peptides as reported in the literature.[23]

Table 1. Designed Peptide Sequences[a]

peptide code no.	sequence
peptide 1	FAM-γAbu-Arg-Gly-Arg-Sar-Arg-Sar-Arg-Gly-Arg-Sar-Arg-NH_2
peptide 2	FAM-γAbu-Arg-Lys(stearyl)-Arg-Sar-Arg-Sar-Arg-Gly-Arg-Sar-Arg-NH_2
peptide 3	FAM-γAbu-Arg-Lys(stearyl)-Arg-Sar-Arg-Sar-Arg-Lys(stearyl)-Arg-Sar-Arg-NH_2
R9	FAM-γAbu-Arg-Arg-Arg-Arg-Arg-Arg-Arg-Arg-Arg-NH_2
stearyl-R9	FAM-γAbu-Lys(stearyl)-Arg-Arg-Arg-Arg-Arg-Arg-Arg-Arg-Arg-NH_2

[a]*N*-Methylglycine or sarcosine, γ-aminobutyric acid, and 5(6)-carboxyfluorescein are abbreviated as Sar, γAbu, and FAM, respectively.

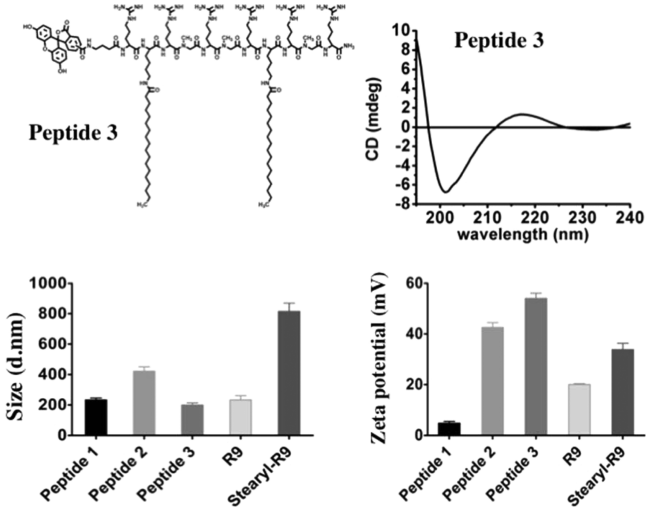

Figure 1. (Top, left) Schematic diagram of peptide 3; (top, right) circular dichroism spectrum of peptide 3 in 25 mM phosphate buffer having pH 7.4. (Bottom) Hydrodynamic size and zeta potential of peptides in water.

Peptide Characterization, Determining Proteolytic Stability of Designed Peptides, and Toxicity Studies of Designed Peptides. The secondary structures of peptides were determined by using circular dichroism (CD) spectroscopy. The CD spectra of peptides 1−3, R9 and stearyl-R9 are shown in Figures 1 and S8. The CD spectra of designed peptides exhibit a minima at ∼200 nm, suggesting unstructured conformation for the peptides.[28] The hydrodynamic diameters of peptide 3 (5 μM), peptide 2 (25 μM), and stearyl-R9 (25 μM) are 199.7 ± 24.7, 421.7 ± 50.4, and 814.3 ± 95.8 nm ,respectively, indicating that, with increasing lipidation, the hydrodynamic size reduces owing to the formation of the more compact structures of the self-assembled lipopeptides (Figures 1 and S9, and Table S2). The magnitude of zeta potential values for peptide 3 (5 μM), peptide 2 (25 μM), and stearyl-R9 (25 μM) in water are +54.1 ± 3.6, +42.6 ± 3.3, and +33.8 ± 4.3 mV, respectively (Figure 1, Table S2). High zeta potential values stabilize the self-assembled peptide 2, peptide 3, and stearyl-R9 due to the presence of electrostatic repulsion among the self-assembled peptide nanostructures.[29] On the other hand, the lower magnitude of zeta potential values for peptide 1 (4.8 ± 1.2 mV) and R9 (20.1 ± 0.6 mV) destabilize the self-assembled peptide 1 and R9, since attractive van der Waal forces induce aggregation among the self-assembled nanostructures of peptides (Figure 1, Table S2).[29] TEM images (Figure 2) and SEM images (Figure S10) reveal the morphology of self-assembled peptide nanostructures.[26,30] TEM images show that the dimensions of lipidated peptide 2, peptide 3, and stearyl-R9 are 74.6 ± 10.9, 13.7 ± 1.4, and 210 ± 49.1 nm, respectively, in water. Proteolytic stability of the cell penetrating peptide is important as it enhances the stability of peptide and peptide−cargo nanocomplexes and also facilitates their cellular internalization at high yield. The protease stability of peptide 3 and stearyl-R9 was tested in the presence of trypsin protease, and the mass of the fragments and intact peptides were checked by MALDI-TOF (Figures S11, S12 and Table 2). Figures S11 and S12 show peptide 3 has much better proteolytic stability than stearyl-R9. Stearyl-R9 is completely cleaved within 30 min, whereas peptide 3 remains intact until 1 h and was cleaved very less until 2 h. This enhanced stability of peptide 3 is crucial for the stability of the peptide3-cargo nanocomplexes and its

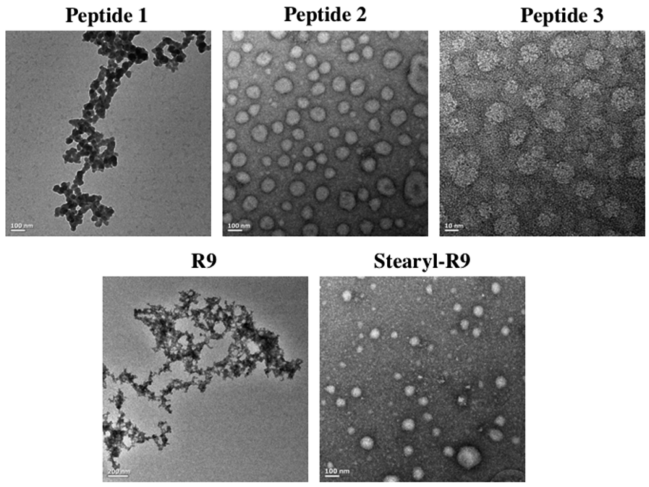

Figure 2. TEM images of peptides.

DOI: 10.1021/acsami.5b04392
ACS Appl. Mater. Interfaces 2015, 7, 18397−18405

Table 2. Identification of Proteolyzed Fragments of Stearyl-R9 and Peptide 3 by MALDI

reaction time (min)	peptide ID	fragments	MW_{calcd} (Da)	MW_{obsd} (Da)
30	stearyl-R9	FAM-γAbu-Lys(stearyl)-Arg-Arg-Arg-Arg-Arg-Arg-Arg-Arg-OH	2105.57	2107.65
		FAM-γAbu-Lys(stearyl)-Arg-Arg-Arg-Arg-Arg-Arg-Arg-OH	1949.38	1950.52
		FAM-γAbu-Lys(stearyl)-Arg-Arg-Arg-Arg-Arg-Arg-OH	1793.19	1794.39
		FAM-γAbu-Lys(stearyl)-Arg-Arg-Arg-Arg-Arg-OH	1637.00	1638.26
		FAM-γAbu-Lys(stearyl)-Arg-Arg-Arg-Arg-OH	1480.81	1482.13
		FAM-γAbu-Lys(stearyl)-Arg-Arg-Arg-OH	1324.62	1326.00
		FAM-γAbu-Lys(stearyl)-Arg-Arg-OH	1168.43	1169.87
		FAM-γAbu-Lys(stearyl)-Arg-OH	1012.24	1013.74
120	peptide 3	Lys(stearyl)-Arg-Sar-Arg-NH_2	794.62	795.69
		FAM-γAbu-Arg-Lys(stearyl)-Arg-Sar-Arg-Sar-Arg-OH	1622.45	1623.13

cellular internalization in high yield. Long-term cytotoxicity on internalization of all the designed and controlled peptides were evaluated using MDA-MB-231 cell line by MTT assay (Figure 3). Peptides 1−3, R9, and stearyl-R9 showed no toxicity until

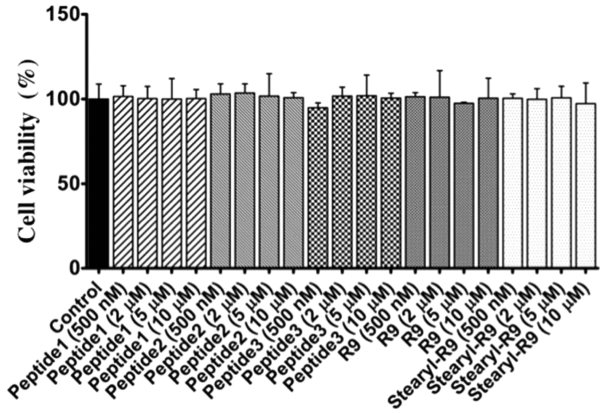

Figure 3. Cytotoxicity analysis of peptides for 48 h time point in MDA-MB-231 cell line. Error bars indicate SD from three separate experiments.

10 μM concentration in the MDA-MB-231 cell line (Figure 3). For all in vitro studies, 5 μM peptides were used to avoid any long-term cytotoxicity arising from the delivery vehicle.

Cellular Uptake Studies of Designed Peptides. The internalization efficiency of the designed FAM-labeled peptides were examined by flow cytometry (Figure 4) and confocal microscopy (Figure 5). The cells were treated with designed peptides for 5 min, 1 h, and 3 h at 37 °C followed by trypsinization and washed twice to remove the cell surface bound peptides and analyzed by flow cytometry (Figure 4). Since flow cytometry does not discriminate between membrane-bound and internalized fluorochrome, cells were trypsinized to remove surface bound FAM labeled peptides.[15]

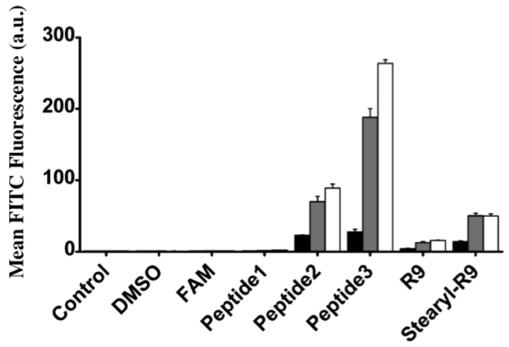

Figure 4. Flow cytometry analysis of time-dependent (5 min, 1 and 3 h) cellular uptake studies of FAM labeled peptides (5 μM) in MDA-MB-231 cells. Error bars indicate SD from three separate experiments. The black, gray, and white bars represent 5 min, 1 h, and 3 h time points, respectively.

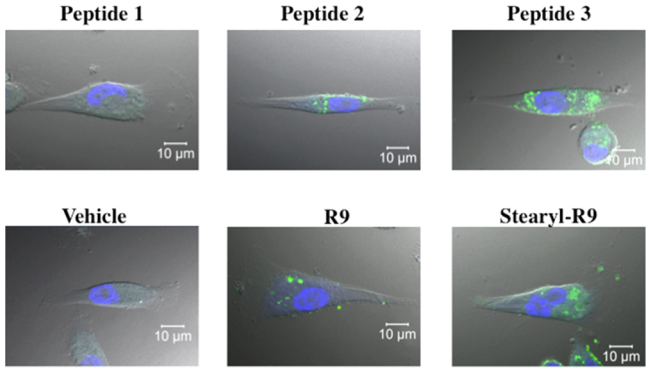

Figure 5. Cellular internalization of FAM labeled peptides in MDA-MB-231 cells. Nuclei are stained with DAPI.

Peptide 3 having two stearyl moieties showed very high internalization efficiency compared to peptide 2 and stearyl-Arg9, indicating that the increased lipidation by longer lipidic moiety contributed significantly in peptide internalization (Figure 4). In this study, we integrated three protein designing components: (a) positively charged residue arginine which could potentially bind with cargo and enhance cellular internalization of peptides by forming stronger bidentate hydrogen bonds with cell surface phosphates, sulfates and carboxylates, (b) unnatural amino acid sarcosine to provide better proteolytic stability and also minimize interpeptide aggregation, and (c) side chain modification by two longer lipidic moieties to facilitate the internalization. It is evident that the increased lipidation by longer lipidic moiety facilitates significantly the internalization of peptides.

Trafficking Pathways of Designed Peptides. To evaluate the effect of energy depletion on cellular uptake, uptake studies of designed peptides were performed in the presence of NaN_3 and 2-deoxy-D-glucose.[16] NaN_3 and 2-deoxy-D-glucose inhibit ATP-dependent pathways by depleting the cellular ATP pool.[16] Figure 6 shows the internalization efficiency of the designed peptides in the presence of NaN_3 and 2-deoxy-D-glucose. The less internalization of peptide 3 in the presence of inhibitors indicates that the peptide 3 is taken up by the cells by both ATP-independent and ATP-dependent pathways.

The confocal images (Figure 5) show punctate patterns of labeling by peptide 3, suggesting uptake via endocytic pathways.[31] The uptake studies of peptide 3 were performed

DOI: 10.1021/acsami.5b04392
ACS Appl. Mater. Interfaces 2015, 7, 18397−18405

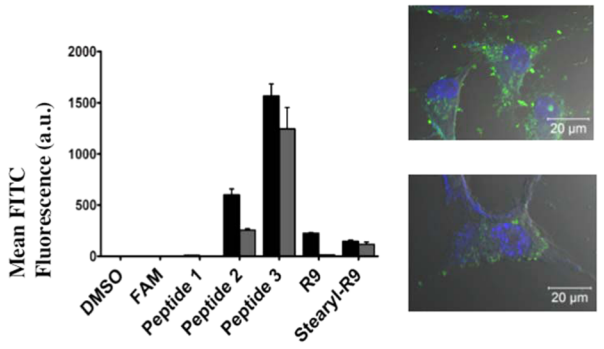

Figure 6. (Left) Flow cytometry data shows the cellular uptake studies of FAM labeled peptides (black colored bars) and FAM labeled peptides in the presence of inhibitors (10 mM NaN_3 and 50 mM 2-deoxy-D-glucose, represented as gray colored bars) in MDA-MB-231 cells. Error bars indicate SD from two separate experiments. (Right, top) Confocal image showing internalization of peptide 3 and (right, bottom) internalization of peptide 3 in the presence of inhibitors, 10 mM NaN_3, and 50 mM 2-deoxy-D-glucose.

in the presence of different inhibitors of endocytosis, chlorpromazine (inhibitor for clathrin), 5-(*N*-ethyl-*N*-isopropyl) amiloride (abbreviated as EIPA, inhibitor for macropinocytosis), nystatin (inhibitor for caveolae), and methyl-β-cyclodextrin (causes cholesterol depletion and inhibitor for caveolae).[9,14,15,32] We also examined the role of actin cytoskeleton in peptide endocytosis by performing uptake studies in the presence of actin polymerization inhibitor, Cytochalasin D.[14]

Figure 7 and Figure S13 show peptide 3 internalization was reduced in the presence of chlorpromazine, EIPA, nystatin, and Cytochalasin D. Interestingly, the internalization of peptide 3 dramatically enhanced in the presence of methyl-β-cyclodextrin (Figure 7), probably suggesting the disruption of membrane structure.[33] In the presence of chlorpromazine and EIPA, the

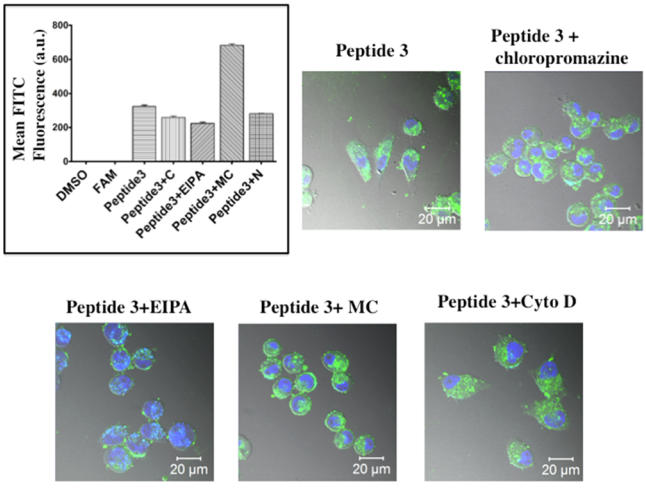

Figure 7. Flow cytometry analysis (inset) and confocal data of cellular uptake studies of peptide 3 in MDA-MB-231 cells in the presence of inhibitors of endocytosis and actin polymerization inhibitor. Inhibitors of endocytosis, chlorpromazine (represented as "C"), methyl-β-cyclodextrin (represented as "MC"), 5-(*N*-ethyl-*N*-isopropyl) amiloride (abbreviated as "EIPA"), and nystatin (represented as "N") and actin polymerization inhibitor cytochalasin D (abbreviated as Cyto D) were used. Error bars in flow cytometry data indicate SD from two separate experiments.

peptide 3 showed less internalization indicating that peptide 3 is internalized by several endocytic pathways (clathrin, macropinocytosis, and caveolae) and actin cytoskeleton may play significant role in its endocytic processes (Figure 7, Figure S13).

Determining the Cargo Internalization by Designed Peptides as a Model Study. We used DY-547 labeled siRNA (siGLO red transfection indicator) as labeled cargo for qualitatively measuring the cargo internalization efficiency of our designed peptides. The transfection efficiency of peptide-cargo complexes significantly depends on the charge, stability and the size of the complexes.[34] Peptide based transporters were used in molar excess over siRNA for forming positively charged complexes, which facilitate cellular internalization. Additionally, such complexation also protects siRNA against nuclease-mediated degradation.[34] Peptide 3 and siRNA were mixed at different molar ratios (1:5−1:100), and the size and zeta potential of the siRNA-peptide 3 nanocomplexes were determined in water (Figures 8a,b and S14, Table S3). Figure

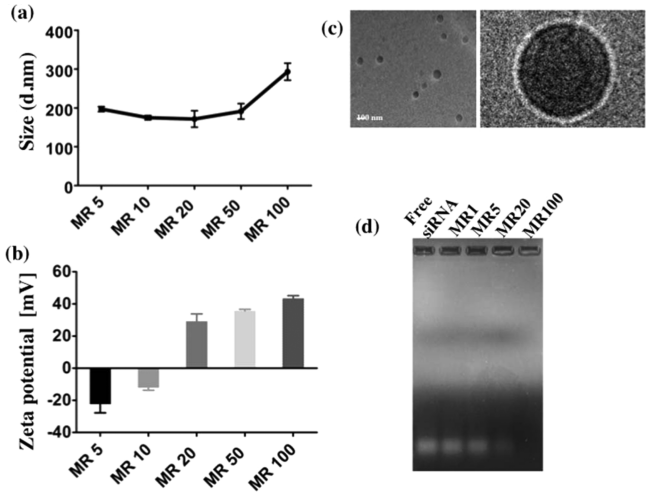

Figure 8. (a) Size of peptide 3−siRNA nanocomplexes at different peptide/siRNA molar ratio (MR); (b) zeta potential of peptide 3−siRNA nanocomplexes at different peptide/siRNA molar ratio (MR); (c) cryo-TEM image of peptide 3−siRNA nanocomplexes at 100:1 molar ratio; and (d) agarose gel retardation assay showing the peptide 3−siRNA complex formation at different molar ratios.

8b reveals with increasing peptide concentration zeta potential of peptide 3-siRNA nanocomplexes increases. At molar ratio 50 and 100, siRNA can be encapsulated well by cationic peptide 3 and such peptide 3-siRNA nanocomplexes are appropriate for cellular internalization. Cryo-TEM data (Figure 8c) reveals 27.7 ± 5.2 nm dimension of siRNA−peptide 3 nanocomplex (1:100 molar ratio) in RNase free water. The hydrodynamic radius and zeta potential value of the (1:100) siRNA−peptide 3 nanocomplexes are 293.3 ± 37.9 nm and +43.4 ± 1.7 mV, respectively (Table S3). The size and zeta potential of peptide−siRNA complexes are described in Figures S14, S15 and Tables S3, S4. The morphology of all the siRNA−peptide complexes was determined by normal TEM (Figure S16) and SEM (Figure S17). Agarose gel shift assay was performed to characterize the interaction between peptide 3 and siRNA (Figure 8d). Figure 8d shows peptide 3−siRNA complexes taken at different molar ratios (abbreviated as MR in the figure), and with increasing cationic peptide concentrations, the band for free siRNA disappeared, suggesting the ionic

DOI: 10.1021/acsami.5b04392
ACS Appl. Mater. Interfaces 2015, 7, 18397−18405

interaction exists between siRNA and cationic lipopeptide. At peptide 3/siRNA molar ratio 100, all the siRNA molecules were encapsulated by peptide 3. The transfection efficiency of FAM-labeled facial peptides was examined in the presence of DY-547 labeled siRNA (siGLO red transfection indicator) at siRNA/peptide molar ratio 1:100. Flow cytometry data (Figure 9)

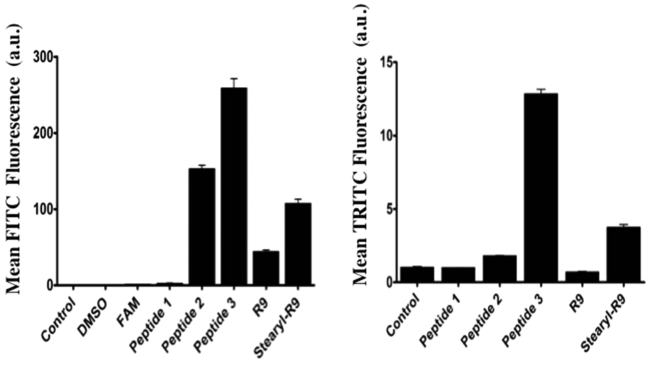

Figure 9. Cellular uptake studies of peptide−siRNA nanocomplexes in MDA-MB-231 cells. Five μM FAM labeled peptides and 50 nM siRNA (DY- 547 labeled siRNA) were taken for each condition. (Left) Mean FITC fluorescence from FAM labeled peptides and (right) mean TRITC fluorescence from DY-547 labeled siRNA. Error bars indicate SD from three separate experiments.

infers peptide 3 has significantly higher transfection efficiency than stearyl-Arg9. In the case of peptide 3, the improved proteolytic stability of the peptide (Figure S12) facilitates the internalization of peptide−cargo complexes (Figures 9 and 10),

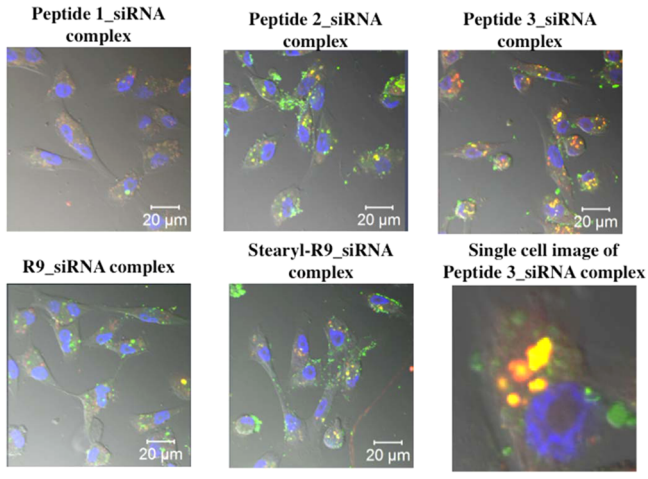

Figure 10. Intracellular trafficking of 5 μM FAM labeled peptides and 50 nM DY-547 labeled siRNA nanocomplexes in MDA-MB-231 cells. Nuclei are stained with DAPI. Single cell image of peptide 3−siRNA complex shows the colocalization of siRNA and peptide 3.

and the intracellular colocalization of FITC and TRITC signal infers the high yield cellular internalization of peptide 3−siRNA nanocomplexes (Figure 10). Time dependent peptide internalization (Figure 4) shows that it takes nearly 1 h for maximum internalization. Peptide 3 has considerable proteolytic stability until 2 h (Figure S12). This enhances the stability of peptide 3 and peptide 3−siRNA nanocomplexes and facilitates the high yield cargo internalization. The enhanced stability of peptide−cargo nanocomplex also sheds light on the different complexation mechanism of cargo with facial lipopeptides and with lipidated oligoarginine peptides. Figure 11 shows the release of peptide 3 and siRNA from the peptide 3−siRNA nano-

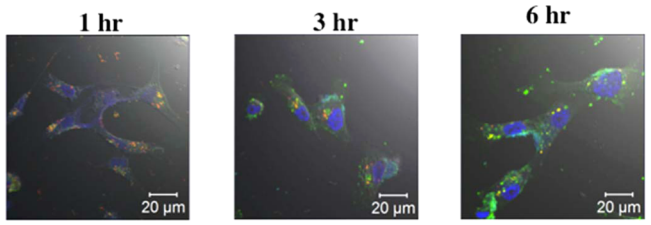

Figure 11. Internalized peptide 3−siRNA nanocomplexes show the release of siRNA and peptide 3 from nanocomplexes at different time points. Nuclei are stained with DAPI.

complexes with time. This evidence infers that the two stearyl moieties facilitate enhanced internalization of peptide−siRNA complexes and the stability of the peptide−siRNA noncovalent nanocomplexes was enhanced by the protease-stability of the carrier peptide. Furthermore, less cationic charge in facial peptides facilitates the unpacking of siRNA−peptide nanocomplexes.

4. CONCLUSIONS

In conclusion, we report that the facial nanostructured lipopeptide, having Arg-Sar-Arg motif and side chain modification with two stearyl moieties, exhibited significantly enhanced cellular internalization of peptide and peptide−cargo nanocomplexes even with only six L-arginine residues. This study infers multifunctional facial lipopeptide having Arg-Sar-Arg motif and two stearyl moieties exhibits higher cargo internalization efficacy than stearylated nona-arginine and can be exploited as a promising drug delivery vehicle for intracellular delivery of biomacromolecules. Additionally, such nanostructured peptide could be potentially translated into clinic as a next-generation drug delivery vehicle.

■ ASSOCIATED CONTENT

Supporting Information

The Supporting Information is available free of charge on the ACS Publications website at DOI: 10.1021/acsami.5b04392.

General scheme of peptide synthesis (Scheme S1), table containing peptide sequences and their mass (Table S1), MALDI mass spectra of peptides (Figures S1−S5), ^{1}H NMR spectrum (Figures S6, S7), CD spectra (Figure S8), particle size distribution of peptides (Figure S9), size and zeta potential values of peptides (Table S2), SEM images of peptides (Figure S10), MALDI-TOF analysis of trypsin digested stearyl-R9 (Figure S11), MALDI-TOF analysis of trypsin digested peptide 3 (Figure S12), flow cytometry analysis in the presence of actin polymerization inhibitor (Figure S13), particle size distributions of peptide-siRNA complexes (Figures S14, 15), size and zeta potential values of peptide-siRNA complexes (Tables S3, S4), normal TEM images of peptide-siRNA complexes (Figure S16), and SEM image of peptide-siRNA complexes (Figure S17) (PDF)

■ AUTHOR INFORMATION

Corresponding Author

*E-mail: rituparna@iiserkol.ac.in.

DOI: 10.1021/acsami.5b04392
ACS Appl. Mater. Interfaces 2015, 7, 18397−18405

Author Contributions

C.D. and R.S.R. have designed the experiments. C.D. has performed the peptide synthesis and characterization, and K.C. and R.S.R. have performed the cell biology experiments. Both C.D. and R.S.R. have contributed to writing the paper.

Notes

The authors declare no competing financial interest.

■ ACKNOWLEDGMENTS

This study is funded by DBT Ramalingaswami (D.No. BT/HRD/35/02/2006), DBT Nanobiotechnology (BT/PR6761/NNT/28/619/2012), and start-up grant received from IISER Kolkata. R.S.R. thanks DBT for Ramalingaswami fellowship, C.D. thanks CSIR for fellowship, and K.C. thanks IISERK for Ph.D. fellowship. The authors thank Dr. Jayasri Das Sarma and Mr. Tanmoy Dolui (IISERK) for flow cytometry data, Mr. Subodh Jain (IISERK mass spec facility) for mass spec data, IISERK Polymer Research Centre for Dynamic Light Scattering facility, Mr. Ritabrata Ghosh (IISERK confocal facility) for confocal data and Mr. Kashinath Sahu (IISERK SEM facility) for SEM data. We thank Dr. Jayati Sengupta, Dr. Umesh Prasad Singh, Mr. Sailen Dey, and Mr. Chiranjit Biswas of IICB, Kolkata for cryo-TEM image reported in this paper and Dr. S Raghothama of NMR research centre of IISc Bangalore for NMR spectra. We thank Mr. Samik Roy Moullick of S.N. Bose TEM facility for normal TEM images.

■ REFERENCES

(1) Mitragotri, S.; Burke, P. A.; Langer, R. Overcoming the Challenges in Administering Biopharmaceuticals: Formulation and Delivery Strategies. *Nat. Rev. Drug Discovery* **2014**, *13*, 655−672.

(2) Yoo, J. W.; Irvine, D. J.; Discher, D. E.; Mitragotri, S. Bio-Inspired, Bioengineered and Biomimetic Drug Delivery Carriers. *Nat. Rev. Drug Discovery* **2011**, *10*, 521−535.

(3) Heitz, F.; Morris, M. C.; Divita, G. Twenty Years of Cell-Penetrating Peptides: From Molecular Mechanisms to Therapeutics. *Br. J. Pharmacol.* **2009**, *157*, 195−206.

(4) Munyendo, W. L.; Lv, H.; Benza-Ingoula, H.; Baraza, L. D.; Zhou, J. Cell Penetrating Peptides in the Delivery of Biopharmaceuticals. *Biomolecules* **2012**, *2*, 187−202.

(5) Wu, C. H.; Chen, Y. P.; Wu, S. H.; Hung, Y.; Mou, C. Y.; Cheng, R. P. Enhanced Non-Endocytotic Uptake of Mesoporous Silica Nanoparticles by Shortening the Peptide Transporter Arginine Side Chain. *ACS Appl. Mater. Interfaces* **2013**, *5*, 12244−8.

(6) Rajendran, L.; Knölker, H. J.; Simons, K. Subcellular Targeting Strategies for Drug Design and Delivery. *Nat. Rev. Drug Discovery* **2010**, *9*, 29−42.

(7) Nakase, I.; Akita, H.; Kogure, K.; Gräslund, A.; Langel, Ü.; Harashima, H.; Futaki, S. Efficient Intracellular Delivery of Nucleic Acid Pharmaceuticals Using Cell-Penetrating Peptides. *Acc. Chem. Res.* **2012**, *45*, 1132−1139.

(8) Shukla, R. S.; Qin, B.; Cheng, K. Peptides Used in the Delivery of Small Noncoding RNA. *Mol. Pharmaceutics* **2014**, *11*, 3395−3408.

(9) Mandal, D.; Nasrolahi Shirazi, A.; Parang, K. Cell-Penetrating Homochiral Cyclic Peptides as Nuclear-Targeting Molecular Transporters. *Angew. Chem., Int. Ed.* **2011**, *50*, 9633−9637.

(10) Lättig-Tünnemann, G.; Prinz, M.; Hoffmann, D.; Behlke, J.; Palm-Apergi, C.; Morano, I.; Herce, H. D.; Cardoso, M. C. Backbone Rigidity and Static Presentation of Guanidinium Groups Increases Cellular Uptake of Arginine-Rich Cell-Penetrating Peptides. *Nat. Commun.* **2011**, *2*, 453.

(11) Qian, Z.; Liu, T.; Liu, Y. Y.; Briesewitz, R.; Barrios, A. M.; Jhiang, S. M.; Pei, D. Efficient Delivery of Cyclic Peptides into Mammalian Cells with Short Sequence Motifs. *ACS Chem. Biol.* **2013**, *8*, 423−431.

(12) Oh, D.; Nasrolahi Shirazi, A.; Northup, K.; Sullivan, B.; Tiwari, R. K.; Bisoffi, M.; Parang, K. Enhanced Cellular Uptake of Short Polyarginine Peptides through Fatty Acylation and Cyclization. *Mol. Pharmaceutics* **2014**, *11*, 2845−2854.

(13) Nasrolahi Shirazi, A.; Oh, D.; Tiwari, R. K.; Sullivan, B.; Gupta, A.; Bothun, G. D.; Parang, K. Peptide Amphiphile Containing Arginine and Fatty Acyl Chains as Molecular Transporters. *Mol. Pharmaceutics* **2013**, *10*, 4717−4727.

(14) Ren, Y.; Hauert, S.; Lo, J. H.; Bhatia, S. N. Identification and Characterization of Receptor-Specific Peptides for siRNA Delivery. *ACS Nano* **2012**, *6*, 8620−8631.

(15) Appelbaum, J. S.; LaRochelle, J. R.; Smith, B. A.; Balkin, D. M.; Holub, J. M.; Schepartz, A. Arginine Topology Controls Escape of Minimally Cationic Proteins from Early Endosomes to the Cytoplasm. *Chem. Biol.* **2012**, *19*, 819−830.

(16) Smith, B. A.; Daniels, D. S.; Coplin, A. E.; Jordan, G. E.; McGregor, L. M.; Schepartz, A. Minimally Cationic Cell-Permeable Miniature Proteins via α-Helical Arginine Display. *J. Am. Chem. Soc.* **2008**, *130*, 2948−2949.

(17) McNaughton, B. R.; Cronican, J. J.; Thompson, D. B.; Liu, D. R. Mammalian Cell Penetration, siRNA Transfection, and DNA Transfection by Supercharged Proteins. *Proc. Natl. Acad. Sci. U. S. A.* **2009**, *106*, 6111−6116.

(18) Lehto, T.; Abes, R.; Oskolkov, N.; Suhorutsenko, J.; Copolovici, D. M.; Mäger, I.; Viola, J. R.; Simonson, O. E.; Ezzat, K.; Guterstam, P.; Eriste, E.; Smith, C. I.; Lebleu, B.; Samir El, A.; Langel, Ü. Delivery of Nucleic Acids with a Stearylated $(RxR)_4$ Peptide Using a Non-Covalent Co-Incubation Strategy. *J. Controlled Release* **2010**, *141*, 42−51.

(19) Mo, R. H.; Zaro, J. L.; Shen, W. C. Comparison of Cationic and Amphipathic Cell Penetrating Peptides for siRNA Delivery and Efficacy. *Mol. Pharmaceutics* **2012**, *9*, 299−309.

(20) Crombez, L.; Aldrian-Herrada, G.; Konate, K.; Nguyen, Q. N.; McMaster, G. K.; Brasseur, R.; Heitz, F.; Divita, G. A New Potent Secondary Amphipathic Cell-Penetrating Peptide for siRNA Delivery into Mammalian Cells. *Mol. Ther.* **2009**, *17*, 95−103.

(21) Langlet-Bertin, B.; Leborgne, C.; Scherman, D.; Bechinger, B.; Mason, A. J.; Kichler, A. Design and Evaluation of Histidine-Rich Amphipathic Peptides for siRNA Delivery. *Pharm. Res.* **2010**, *27*, 1426−1436.

(22) Futaki, S.; Suzuki, T.; Ohashi, W.; Yagami, T.; Tanaka, S.; Ueda, K.; Sugiura, Y. Arginine-Rich Peptides. An Abundant Source of Membrane-Permeable Peptides Having Potential as Carriers for Intracellular Protein Delivery. *J. Biol. Chem.* **2001**, *276*, 5836−5840.

(23) Futaki, S.; Ohashi, W.; Suzuki, T.; Niwa, M.; Tanaka, S.; Ueda, K.; Harashima, H.; Sugiura, Y. Stearylated Arginine-Rich Peptides: A New Class of Transfection Systems. *Bioconjugate Chem.* **2001**, *12*, 1005−1011.

(24) Rothbard, J. B.; Kreider, E.; VanDeusen, C. L.; Wright, L.; Wylie, B. L.; Wender, P. A. Arginine-Rich Molecular Transporters for Drug Delivery: Role of Backbone Spacing in Cellular Uptake. *J. Med. Chem.* **2002**, *45*, 3612−3618.

(25) Rothbard, J. B.; Jessop, T. C.; Wender, P. A. Adaptive Translocation: The Role of Hydrogen Bonding and Membrane Potential in the Uptake of Guanidinium-Rich Transporters into Cells. *Adv. Drug Delivery Rev.* **2005**, *57*, 495−504.

(26) Li, M.; Liu, P.; Gao, G.; Deng, J.; Pan, Z.; Wu, X.; Xie, G.; Yue, C.; Cho, C. H.; Ma, Y.; Cai, L. Smac Therapeutic Peptide Nanoparticles Inducing Apoptosis of Cancer Cells for Combination Chemotherapy with Doxorubicin. *ACS Appl. Mater. Interfaces* **2015**, *7*, 8005−12.

(27) Rajasekhar, K.; Suresh, S. N.; Manjithaya, R.; Govindaraju, T. Rationally Designed Peptidomimetic Modulators of Aβ Toxicity in Alzheimer's Disease. *Sci. Rep.* **2015**, *5*, 8139.

(28) Kelly, S. M.; Jess, T. J.; Price, N. C. How to Study Proteins by Circular Dichroism. *Biochim. Biophys. Acta, Proteins Proteomics* **2005**, *1751*, 119−139.

DOI: 10.1021/acsami.5b04392
ACS Appl. Mater. Interfaces 2015, 7, 18397−18405

(29) Honary, S.; Zahir, F. Effect of Zeta Potential on the Properties of Nano-Drug Delivery Systems - A Review (Part 2). *Trop. J. Pharm. Res.* **2013**, *12*, 265−273.
(30) Liu, L.; Xu, K.; Wang, H.; Tan, P. K.; Fan, W.; Venkatraman, S. S.; Li, L.; Yang, Y. Y. Self-Assembled Cationic Peptide Nanoparticles as an Efficient Antimicrobial Agent. *Nat. Nanotechnol.* **2009**, *4*, 457−63.
(31) Nakase, I.; Niwa, M.; Takeuchi, T.; Sonomura, K.; Kawabata, N.; Koike, Y.; Takehashi, M.; Tanaka, S.; Ueda, K.; Simpson, J. C.; Jones, A. T.; Sugiura, Y.; Futaki, S. Cellular Uptake of Arginine-Rich Peptides: Roles for Macropinocytosis and Actin Rearrangement. *Mol. Ther.* **2004**, *10*, 1011−1022.
(32) Duchardt, F.; Fotin-Mleczek, M.; Schwarz, H.; Fischer, R.; Brock, R. A Comprehensive Model for the Cellular Uptake of Cationic Cell-Penetrating Peptides. *Traffic* **2007**, *8*, 848−866.
(33) Zidovetzki, R.; Levitan, I. Use of Cyclodextrins to Manipulate Plasma Membrane Cholesterol Content: Evidence, Misconceptions and Control Strategies. *Biochim. Biophys. Acta, Biomembr.* **2007**, *1768*, 1311−1324.
(34) van Asbeck, A. H.; Beyerle, A.; McNeill, H.; Bovee-Geurts, P. H.; Lindberg, S.; Verdurmen, W. P.; Hallbrink, M.; Langel, U.; Heidenreich, O.; Brock, R. Molecular Parameters of siRNA-Cell Penetrating Peptide Nanocomplexes for Efficient Cellular Delivery. *ACS Nano* **2013**, *7*, 3797−807.

DOI: 10.1021/acsami.5b04392
ACS Appl. Mater. Interfaces 2015, 7, 18397−18405